ELSEVIER

Journal of Photochemistry and Photobiology A: Chemistry 102 (1996) 21–28

Journal of PHOTOCHEMISTRY AND PHOTOBIOLOGY A:CHEMISTRY

The dynamics of photodissociation reactions in solution

N. Pugliano *, S. Gnanakaran, Robin M. Hochstrasser

Department of Chemistry, 231 S. 34th Street, University of Pennsylvania, Philadelphia, PA 19104, USA

Abstract

Elementary photoreactions were examined in solution by femtosecond absorption spectroscopy. The transition state properties, energy and coherence transfer into product molecules, various solvent-mediated relaxation mechanisms and influence of solvent diffusion in governing reaction rates are discussed. Two types of reaction are presented. The first involves the impulsive photodissociation of HgI_2 in a solution of ethanol and the second demonstrates how condensed phase hydrogen abstraction processes differ from those in the gas phase.

Keywords: Dynamics; Photodissociation reactions; Solution

1. Introduction

Time-resolved studies of reactive small molecules in solution present a number of opportunities relating solvent-mediated reaction dynamics to condensed phase theories. Predictive models are not currently available for even the simplest systems, because of the complex nature of the solvent dynamics which influence numerous factors during the course of condensed phase chemical reactions. This is easily illustrated by comparing the differences between solution and gas phase reactions. One striking example has been noted for condensed phase hydrogen abstraction reactions [1,2], in which the pseudo-first-order reaction rate constant is found to be at least tenfold slower in solution relative to the analogous gas phase abstraction process! Some of this work is discussed below to illustrate the clear evidence of contributing solute–solvent forces in modifying solvated reactive processes relative to those of the gas phase.

The impulsive photodissociation of simple triatomic molecules into atom–diatom products also provides excellent prototypes through which the details of ultrafast reaction dynamics in solutions can be further explored. In this work, the photodissociation of mercuric iodide in alcohol solutions is considered [3–5]. This particular reaction is known from the analogous gas phase reaction to produce HgI molecules, that are in highly non-equilibrium coherent states, as products [6–8]. Unlike the situation for the gas phase reaction, the presence of a solvent gives rise to energy transfer to and from the solvent modes. It also plays a dominant role in the energy release mechanisms near the transition state and as the reaction products proceed towards thermal equilibrium. Furthermore, the inherent phase coherence throughout the ensemble of generated HgI products is altered through the coupling to the bath of solvent states. Solvent-induced modifications of the potential energy surfaces may also be influential in altering reactive trajectories, as well as the product state partitioning of energy. All of these solvent frictional effects can be addressed by monitoring the details of both the population and coherence relaxation associated with the vibrational and electronic levels involved. Finally, it is particularly interesting to study HgI_2 in a solution of polar molecules, because during the reactive process the non-polar neutral molecule rapidly evolves into polar diatomic and atomic iodine product fragments. This involves charge transfer from the iodine atom, which is released on dissociation to form the polar HgI molecule. This charge switching event which accompanies this reaction obviously couples to the degrees of freedom of the polar solvent molecules [9]. Such a situation permits an opportunity to evaluate whether the solvent adiabatically couples to the reactive motion or whether its response is too slow, thus generating a highly non-equilibrated transient solvent state.

2. Experimental details

The femtosecond spectrometer used to conduct these experiments is based on the 20 Hz Nd:YAG amplification of a colliding pulse mode-locked (CPM) laser. Preamplified CPM light is variably attenuated and imaged into a short (approximately 1 cm) piece of optical fiber to form a white light continuum, which is used to seed a three-stage power

* Corresponding author.

PII S1010-6030(96)04375-0

amplifier. The amplified laser beam is then passed through a series of pulse compression stages to achieve 19 fs pulses. This compressed beam is separated into two parts. One portion is frequency doubled in a 50 μm slice of β-barium borate crystal (BBO) to produce a UV pump beam centered at 320 nm. The cross-correlation of the 320 nm beam with the 19 fs 620 nm pulse characterizes the UV pulse width to be 38 fs. The second portion of the 620 nm beam is variably delayed and focused into an ethylene glycol jet to generate a second white light continuum. Spectral selection of a particular probe wavelength is accomplished with 10 nm wide interference filters. The probe light is split into two equal portions which serve as signal and reference beams, each of which is detected with photodiodes. The photodiode signals are processed with boxcar integration and the results are stored in units of ΔOD (OD, optical density). The sample for these experiments consisted of a 0.5 mm flowing jet of an ethanol solution containing HgI_2 at a concentration of 10 mM.

3. HgI vibrational dynamics: results and models

HgI wavepacket dynamics, characterized through oscillatory signal components, have been observed throughout the spectral region from 380 nm to 560 nm. Three representative magic angle signals of HgI_2 photolysis in ethanol are shown in Fig. 1 for probe wavelengths of 400, 490 and 540 nm. It is apparent from Fig. 1 that the three transients exhibit distinct oscillation frequencies, modulation depths and decay rates. Each of the transients was fitted to a phenomenological multiexponential molecular response function which was convoluted with a gaussian instrument function. The oscillatory portion of the signal was modeled by a term that took the form $B\exp[k_b t]\cos\{\omega t+\phi\}$. The decay constant k_b represents the apparent dephasing rate of the oscillations, ω is the oscillation frequency and ϕ is the phase factor. The wavelength dependence of the fitted beat frequencies and dephasing rates is shown throughout the probed spectral region in Fig. 2.

In the experiments reported here, each molecule of HgI is produced as a superposition of vibrational eigenstates on its X-potential function by pumping HgI_2 with femtosecond pulses. As a result, there is an observable ensemble coherence or oscillating macroscopic polarizability which is related to the vibrational dynamics of the diatomic product fragments. The polarizability is detected through time-resolved electronic absorption spectroscopy as a periodic variation of the transmitted probe field-induced macroscopic polarization. The HgI superposition state is composed of a wide distribution of vibrational eigenstates which all possess a distinct phase relationship with respect to one another. If the probe laser is chosen to interrogate mainly a small fraction of eigenstates within the wavepacket, the oscillatory portion of the transient signal is representative of the dynamics of these vibrational levels. This is illustrated in Fig. 1 by the three vertical transitions which give rise to the transient absorption

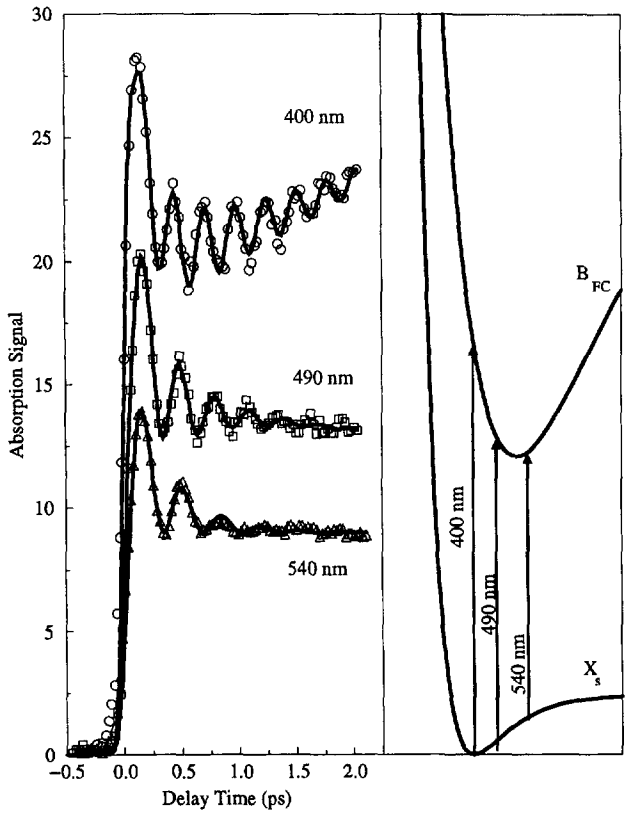

Fig. 1. Three transients, recorded under magic angle conditions, are shown. The prominent oscillatory portion of the signals is indicative of the HgI ground state wavepacket dynamics. The regions of HgI bond lengths which mainly contribute to each of the signals are indicated by the transition arrows. This shows that the lower energy probes interrogate higher vibrational quantum levels in the ground state of HgI. Probing throughout the spectral band of the HgI absorption gives rise to the variation of the oscillatory frequency and decay rate with the probe wavelength.

signals at the specified probe wavelengths. This provides an opportunity to examine vibrational level-dependent solvent-induced relaxation dynamics. According to the conventional models for dephasing, the relaxation rates responsible for phase dissipation in the ensemble should increase with the HgI vibrational quantum number. This is experimentally indi-

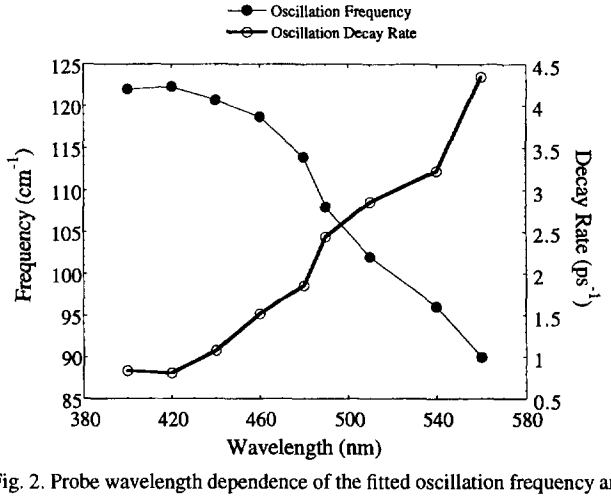

Fig. 2. Probe wavelength dependence of the fitted oscillation frequency and decay rate.

cated by examining the dephasing rate dependence on the probe wavelength in Fig. 2. This verifies that probed level pairs lying high in the HgI anharmonic potential dephase much faster than those low in the well. The reasons for this are reviewed below. Since the wavepacket is formed through an impulsive chemical reaction, the probe wavelength dependence of the transients should also be representative of the details of the reaction dynamics, the product state energy distribution, the properties of the transition state, the time evolution of the reactive and product state potential surfaces and the relaxation of excess energy and phase within the ensemble of product fragments. The characterization of these dynamics leads to an understanding of the force existing between the reactive species and the solvent.

In describing the HgI vibrational phase and energy relaxation dynamics, it is assumed that the reaction is completed on a timescale that is short compared with the available time resolution. The HgI wavepacket generated through the impulsive photolysis of HgI_2 is defined by simply projecting the superposition state onto the primitive HgI vibrational basis functions $|n\rangle$ through $|\Psi(0)\rangle = \Sigma_n C_n|n\rangle$. C_n is the weighting coefficient for the nth eigenstate making up the wavepacket at time zero. These coefficients permit the full density matrix at time zero $\rho_{mn}(0)$ to be defined. The density matrix elements for which $m=n$ account for the pure population dynamics of the level n, and coherence between the level pair (m,n) is defined when $m \neq n$. The time evolution of ρ can be determined through the equation of motion for a multilevel system using perturbation theory [10–12]

$$\dot{\rho}_{mn}(t) = -\frac{i}{\hbar}[H_0, \rho(t)]_{mn} + \sum_{m',n'} \Gamma_{mnm'n'}\rho_{m'n'}(t) \quad (1)$$

The commutator between the system hamiltonian and the density matrix represents the free propagation under the influence of H_0, and the level pair-dependent relaxation rates are $\Gamma_{mnm'n'}$. A common simplification of Eq. (1) arises by considering the coupling of a two-level system to a bath. It involves considering only relaxation matrix elements $\Gamma_{mnm'n'}$ that can be more simply designated as $-\Gamma_{mn}$. These decay rates are often defined as $\Gamma_{mn} = 1/2(\Gamma_{nn} + \Gamma_{mm}) + \Gamma'_{mn}$. The population decay rates out of the levels n and m are Γ_{nn} and Γ_{mm} respectively and Γ'_{mn} is the pure dephasing rate of the ensemble. In this approximation, each density matrix element propagates in time with a complex frequency Ω_{mn} according to

$$\dot{\rho}_{mn}(t) = \rho_{mn}(0)\exp[-(i\omega_{mn} + \Gamma_{mn})t] \quad (2)$$

The remaining $\Gamma_{mnm'n'}$ terms that are excluded from Eq. (2) involve coupling the density matrix element $\rho_{mn}(t)$ to all other $\rho_{m'n'}(t)$. These are known to be important under certain conditions; however, in the present discussion, only those that account for phase preserving population exchange and take a coherently prepared level pair (m,n) to $(m-1,n-1)$ will be considered. Coherence transfer processes are directly obtained from the quantum mechanical relaxation matrix [12] or via Redfield theory [10,11]. The dominant contributions to this coherence transfer process are readily added via the master equation for coherence [12] for a relaxing harmonic system linearly coupled to a bath

$$\begin{aligned}\dot{\rho}_{mn+m}(t) = -1/T_1\{&[(2n+m) + (2n+m+2)\\ &\times\exp(-\beta\hbar\omega)]\rho_{n,n+m}(t) - 2[(n+1)\\ &\times(n+m+1)]^{1/2}\rho_{n+1,n+m+1}(t) - 2[(n)\\ &\times(n+m)]^{1/2}\rho_{n-1,n+m-1}(t)\exp(-\beta\hbar\omega)\}\end{aligned} \quad (3)$$

The first term accounts for coherence decay by upward and downward flow of population. The second and third terms reinforce the coherence of the $(n,n+m)$ level pair due to concerted population flow from level pairs above and below. T_1 in the prefactor is the energy relaxation time of the harmonic oscillator. Eq. (3) shows that coherences are being created and destroyed on the same timescale by the population flow. Therefore the net rate of coherence loss is much slower than predicted by the two-level system approach.

The construction of the full density matrix at a time t can be used to form the probability distribution function $P(r,t)$ of the wavepacket at position r at that time through

$$P(r,t) = \langle r|\Psi(t)\rangle\langle\Psi(t)|r\rangle = \Sigma_{mn}\phi^*_m(r)\phi_n(r)\rho_{mn}(t) \quad (4)$$

where $H_0\phi_n(r) = \hbar\omega_n\phi_n(r)$ is the stationary Schrodinger equation for the anharmonic oscillator. $P(r,t)$ is probed at each time with the limited spectral bandwidth of each femtosecond probe used in the experiment by exciting HgI to its higher lying solvent-modified B electronic state. The comparison between theory and experiment will lead to the characterization of the two-level system damping parameters or more generally those of Eq. (1).

After the phase coherence in the system is completely lost, the ensemble of HgI molecules remains in a vibrationally hot distribution which can be characterized by its diagonal density matrix at each time. The evolution of this non-equilibrated population distribution gives rise to signal variations which show a wavelength dependence indicative of the population shifting amongst the HgI vibrational levels as the molecule loses energy and approaches thermal equilibrium. The signature of this relaxation is found in the longer time portion of the transient absorption signals. For example, scanning out to longer times (more than 2 ps) with a 420 nm probe reveals a transient absorption feature which rises to a maximum at a delay time of 3 ps, followed by a decay to a nearly constant signal level on a timescale of approximately 10 ps. This is illustrated in Fig. 3. As the probe is tuned to lower frequency, this time-resolved absorption shifts to earlier pump–probe time delays, and its decay to a constant signal level occurs more rapidly. Different portions of the vibrationally hot distribution of product molecules, generated through the dissociation reaction, are interrogated with different probe frequencies. As for the coherent portions of the signals, low energy probes sample high energy portions of

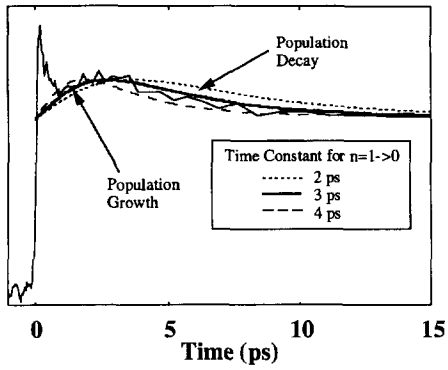

Fig. 3. Longer time portion of the HgI transient response characterizing the evolution of vibrational energy flow from high lying levels towards thermal equilibrium. These data were simulated using the master equation models described in the text, and the results are shown for time constants of 2 ps (- - -), 3 ps (———) and 4 ps (– – –).

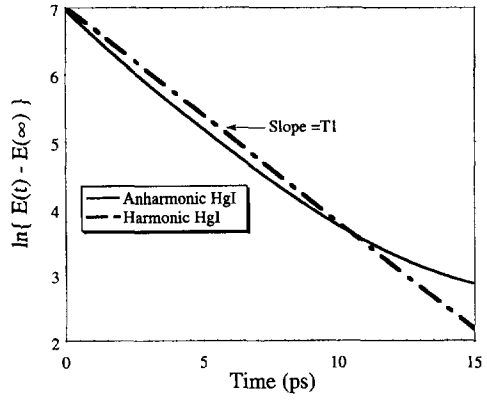

Fig. 4. Energy decay for a harmonic HgI molecule compared with that of anharmonic HgI.

the HgI population distribution, whereas high energy probes provide information on the low energy vibrational states of the well. The expected fast population relaxation for levels high in the well is shown by the long-wavelength probe signals which exhibit an early time transient absorption that rapidly decays [4]. This energy relaxation from high lying levels feeds the lower levels on a picosecond timescale, and this is detected with short-wavelength probes as a rising signal which peaks and then subsequently decays slowly to an equilibrated signal level. These dynamics were modeled with a population master equation which incorporated the anharmonicity of the HgI solute and a density of solvent states described by the power spectrum of neat ethanol [4]. The master equation was based on the assumption that the solute vibrational energy is transferred into the solvent vibrational modes. Simulated molecular responses are superimposed on the data shown in Fig. 3 for the $n'' = 1 \rightarrow 0$ relaxation times of 2, 3 and 4 ps. All of the wavelength-dependent data were reproduced best with the 3 ps value. The influence of the anharmonicity on the energy relaxation is illustrated by the non-exponential decay of the total energy out of the HgI system shown in Fig. 4. This plot is compared with the energy relaxation out of harmonic HgI, possessing a fundamental frequency of 125 cm^{-1}. The simulations of the data also provide an estimate of the initial excess energy of the HgI produced by photodissociation. The best fits were accomplished when the population distribution was centered at $n'' = 10$, corresponding to a total excess vibrational energy of approximately 1050 cm^{-1}. The simulation yields a complete set of state-to-state vibrational relaxation rates between all possible vibrational level pairs. As indicated above, these rates are important in describing the coherence dephasing from the perspective of the two-level system model, as well as the more general model which includes coherence transfer processes. They will be used as input to describe the coherence decay.

3.1. Simulations of the wavepacket dynamics

After a wavepacket is launched, it begins to oscillate at the $N(N-1)/2$ Bohr frequencies of the eigenstate distribution weighted according to their contribution to the superposition state. All of these natural frequencies for the isolated molecule are represented in the waveform probed by the femtosecond pulse. The dephasing of the wavepacket propagating on the HgI surface is partially influenced by the phase mismatches from the different Bohr frequencies for the level pairs contributing to $|\Psi(t)\rangle$. This spreading of the wavepacket represents an irreversible coherence loss process. In the solution phase, there also exists additional, presumably irreversible, dephasing. The models for coherence loss naturally incorporate all of these processes.

A comparison of the data with the simulations shows that the simplified two-level system model for which the coherence loss is described by the rate expression, $\Gamma_{mn} = 1/2(\Gamma_{nn} + \Gamma_{mm}) + \Gamma'_{mn}$, is inadequate to represent our observations and, as expected for systems consisting of nearly equally spaced levels, all of the terms of Eq. (1), including coherence transfer, are required to describe the data appropriately. The evidence supporting this claim is now presented.

3.2. Two-level system coupled to a bath

Simulations of the signal using the model of uncoupled two-level systems were first calculated by neglecting pure dephasing and incorporating only the diagonal density matrix elements (the elements that govern the population transfer from state m to state n) obtained from the vibrational relaxation master equation [4]. In other words, the dephasing rate of a level pair Γ_{mn} was calculated by considering only the average population decay out of these states through $\Gamma_{mn} = 1/2(\Gamma_{nn} + \Gamma_{mm})$. The inclusion of the pure dephasing component Γ'_{mn} only serves to speed up the coherence decay times. Although the wavelength-dependent trends of the oscillation frequency and the decay rates of Fig. 2 are followed, the calculated coherence loss is on the 250 fs timescale. This is much more rapid than observed for the short-wavelength probes. In order to reproduce the dephasing of the oscillations using Eq. (2), the rate of depletion of the population in the nth level needs to be multiplied by a factor of $n/8$. These rates are much slower than the population decay rates of Ref. [4] for the lower levels. The adjustment is

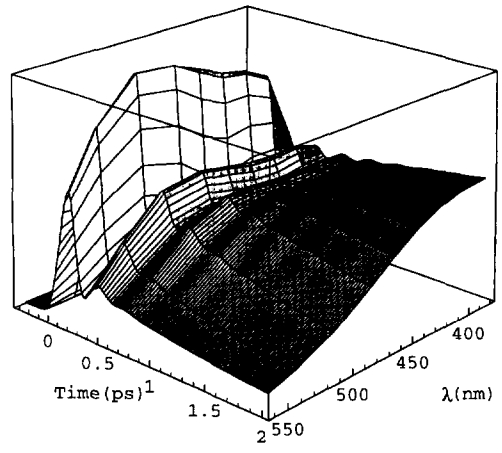

Fig. 5. Simulated transient responses for the two-level system model.

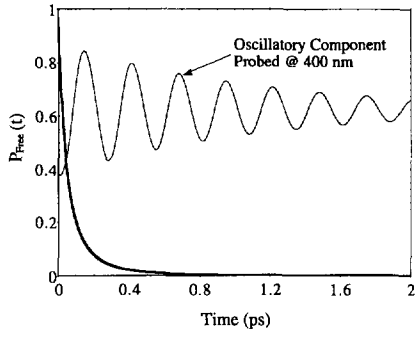

Fig. 6. "Memory" function for the freely propagating wavepacket. The rapid decay is faster than the coherence loss of the low energy vibrational levels.

needed because the coherence is maintained in the lower levels for much longer than predicted by Eq. (2), as can be seen by comparing the plotted rates of Fig. 2 with the persistence of the oscillations in Fig. 5. Furthermore, the fast relaxation from higher lying quantum states tends to cause the overall calculated wavepacket frequency to increase with time, indicating that a single frequency fit is not fully appropriate in considering the observed oscillatory signal components.

The probability $P_{\text{Free}}(t)$ for the wavepacket to have retained its free motion character after a time t is $\langle \Psi(0) \mid \rho(t) \mid \Psi(0) \rangle$, which leads to

$$P_{\text{Free}}(t) = \Sigma_{nm} \rho_{nm}(0) \exp(-\Gamma_{nm} t) \quad (5)$$

In Fig. 6, the "memory" of the freely propagating wavepacket given by Eq. (5) exhibits a rapid non-exponential decay which decays within one cycle of the vibrational motion using the empirically adjusted dynamics. This is much faster than the decay of the oscillations in the pump–probe data represented graphically in Fig. 2. The rapid non-exponential decay of $P_{\text{Free}}(t)$ establishes that the dephasing dynamics of a wavepacket in the condensed phase are not fully described by associating a single "mean" exponential decay function with the freely propagating wavepacket which would exist for the isolated molecule situation.

3.3. Incorporation of coherence transfer

The experimentally measured population dynamics provide a value of 3 ps for the $n'' = 1 \rightarrow 0$ relaxation time. If the oscillator were harmonic, this would be the T_1 relaxation time for the system and would determine the amount of energy in the HgI oscillator at each instant. According to the conventional models for dephasing, the relaxation rates responsible for phase dissipation in the ensemble should increase with the HgI vibrational quantum number. For example, if a harmonic solute which is linearly coupled to a bath of harmonic oscillators is considered, the state-to-state population decay rate is proportional to the quantum number; therefore, at $n = 15$, the relaxation time out of that level is expected to be approximately 200 fs. The transient probed at 540 nm is indicative of levels in this region of the HgI potential. Combining this relaxation process with a pure dephasing effect, the coherence decay timescales would be predicted to lie in the sub-100 fs range for level pairs one-third of the way up the HgI potential. This represents a severe discrepancy between the two-level system model and the experimental results. This discrepancy is not unexpected when the population dynamics assume an important role in the dephasing. The significant effect of these terms can be seen from the following simple argument. Let us consider the coherence in the level pair $(n,n-1)$. The population relaxations from $n \rightarrow n-1$ and from $n+1 \rightarrow n$ occur with approximately the same rate constants if $n \gg 1$. If $\omega_{n+1,n} \approx \omega_{n,n-1}$, relaxation from levels n and $n+1$ to levels $n-1$ and n will not significantly alter the ensemble coherence oscillating at the frequency $\omega_{n+1,n}$. If the pure dephasing is slow compared with this relaxation, there will be no loss of coherence during this population exchange process. This means that the time-dependent displacement of the system $\langle Q \rangle(t)$ will not be significantly altered during the relaxation. In the case of HgI, the population decay times are ultrafast for high quantum numbers [4] and these may exceed the pure dephasing times arising from the adiabatic energy fluctuations. In this limit, it is straightforward to use known principles [12] and implement Eq. (1) together with Eq. (3) to obtain the ensemble coherence. A consideration of the terms in Eq. (1) which transfer coherence indicates that, when the population relaxation rates are large and the frequency of the vibration is low enough compared with $k_B T$ (to allow significant probability for upward transitions to occur), the coherence will be maintained longer than expected from the approximation of the two-level system. Our data appear to be in accord with the simple theoretical prediction of Eq. (3).

In Fig. 7, the results are shown for the propagation of a wavepacket centered at 2.65 Å based on the full population master equation of Ref. [4] combined with the coherence transfer dynamics of Eq. (3). An additional energy-independent pure dephasing rate of $1/T'_2 = 0.5\ \text{ps}^{-1}$ for adjacent level pairs is included to bring the theory more into line with the experimentally observed dephasing rates. Non-adjacent level pairs were ascribed a pure dephasing rate of $|n-m|^2/$

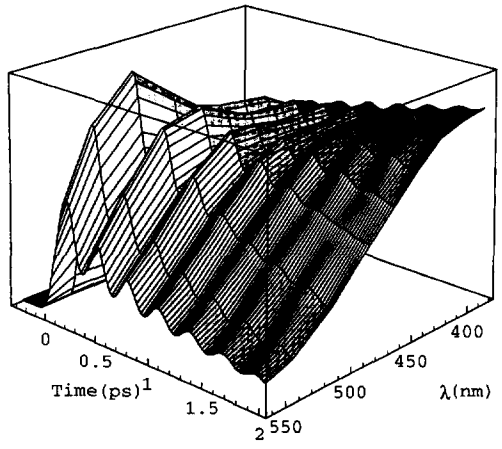

Fig. 7. Simulated transient responses for the model which includes the full population master equation, the coherence transfer terms and an energy-independent pure dephasing time of 2 ps.

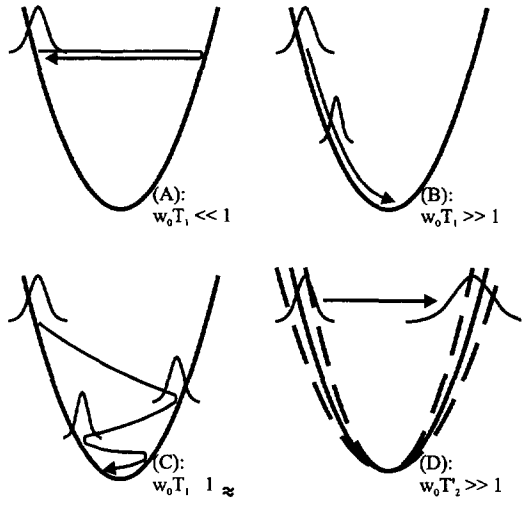

Fig. 8. Classical analogies of wave packet dynamics. (A) Free motion; coherence transfer in overdamped (B) and underdamped (C) limit; (D) pure dephasing.

T'_2. Compared with the simulation of Fig. 5, the oscillations persist for much longer times on inclusion of coherence transfer terms. The short-wavelength probes are found to be consistent with the observed data without further adjustment. The population relaxation transfers coherence between these level pairs, and oscillations persist for times longer than those predicted by the two-level propagator for probes that interrogate these level pairs. The longer wavelength probe signals do not dephase as fast as the observations, indicating that the pure dephasing is most probably energy dependent. Because each of the N level pairs dephases at different rates, the average energy $\langle E(t) \rangle$ of the eigenstates composing the wavepacket decreases with time, and this represents the relaxation of the initial phase of the molecular system. In summary, coherence transfer terms are important for the retention of coherence in the lower levels, and pure dephasing must be energy dependent to yield a more rapid decay of the oscillations interrogated with the long-wavelength probe.

In many respects, wavepacket dynamics can be more naturally discussed in terms of the coordinate basis. Within the picture, the classical analogy between wavepacket motion illustrated in Fig. 8(a) and classical particle-like behavior can be made. Clearly, the unperturbed oscillatory motion of the wavepacket state can be thought of as a classical ball or spatial distribution of balls moving on a frictionless harmonic potential well. These analogies can also be useful when relaxation plays a role in the dynamics. This is easily carried out theoretically for the case of Brownian motion by using the Green's function $G(r,t|r_0,v_0)$ of Chandrasekhar [13] to propagate the classical position distribution $P(r_0,v_0)$ so that

$$P(r,t) = \int dr_0\, G(r,t|r_0,v_0)P(r_0,v_0) \qquad (6)$$

The results are very similar indeed to those obtained from quantum mechanics. For example, in the strongly overdamped limit, a distribution on the potential surface moves towards its equilibrated resting position without any possibility for the existence of recurrences. If energy relaxation in the system is fast compared with the coherence loss time and the oscillation period, the packet can essentially slide down one side of the potential while retaining a narrow distribution in r. This is illustrated in Fig. 8(b) and is considered to be important for the high energy level pairs (above $n=15$) in the HgI system. If the packet loses energy on a timescale that is slower than the oscillation period, the wavepacket would exhibit recurrences during the relaxation. This situation corresponds to a moderately damped particle oscillating on its harmonic surface, and is illustrated in Fig. 8(c). In the eigenstate basis, both of these possibilities correspond to coherence transfer under different relaxation conditions. Even pure dephasing can be thought of from a classical point of view. The nature of adiabatic dephasing originates in the stochastic energy fluctuations imparted by the bath on the potential energy of the system. This serves to introduce random uncorrelated fluctuations of the energy of the coherently prepared level pairs throughout the ensemble. So, in one part of the solution, a bath fluctuation exerts a force on the system which makes its potential more shallow, whereas in another portion of the ensemble, a bath fluctuation serves to tighten the potential. The effect of these random forces on the ensemble average of the coherence is to delocalize the distribution of position eigenstates, and this is illustrated in Fig. 8(d).

As demonstrated above, the fast population relaxation in HgI is critical to the description of the dephasing dynamics, as well as being important for understanding activated processes in the condensed phase. Furthermore, the fast timescales are comparable with vibrational relaxation dynamics for molecular ions in polar solutions, indicating that the forces on the vibrational coordinate are large. For these reasons, classical molecular dynamics simulations were employed to calculate the vibrational relaxation of HgI and to determine the nature of the solvent forces involved. The simulations yielded the classical force–force autocorrelation function for HgI in ethanol. This function is defined by the high temperature version of the friction spectrum through the familiar Landau–Teller expression for T_1 as [14]

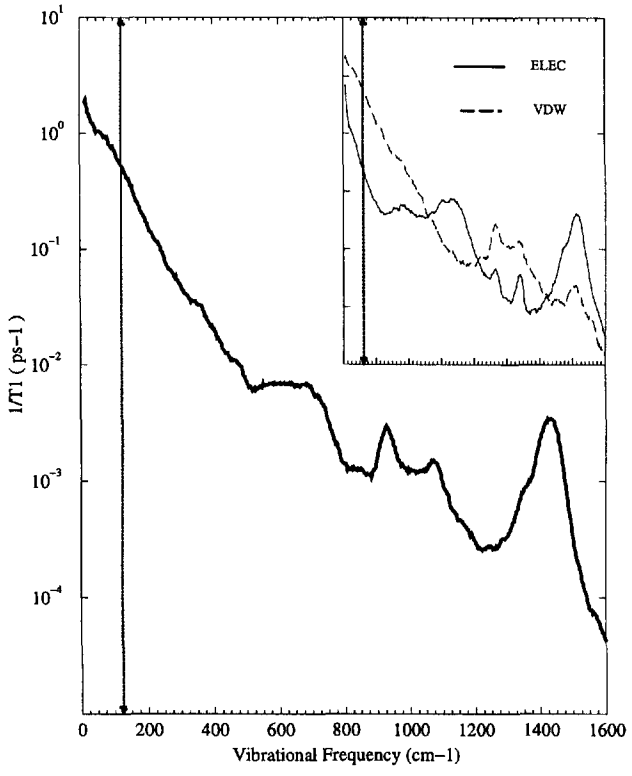

Fig. 9. Frequency-dependent friction spectrum of the solvent force projected onto the HgI bond.

$$\frac{1}{T_1} = \frac{\zeta_{cl}(\omega)}{\mu} \tag{7}$$

in which T_1 is the fundamental relaxation time, μ is the reduced mass and $\zeta_{cl}(\omega)$ is the frequency-dependent friction. The simulation consisted of an HgI diatomic and 255 ethanol molecules with periodic boundary conditions. The charge distribution for polar HgI was obtained via ab initio calculations. The ground state solvated potential of mean force was calculated and was found to be approximately 7% deeper than that of the gas phase. This is consistent with the fact that the measured oscillation frequencies presented in Fig. 2 are similar to those of the isolated molecule. All the molecular dynamics simulations were carried out using CHARMM [15], in which the HgI bond was constrained to its gas phase equilibrium value using SHAKE. The calculated force–force spectrum is shown in Fig. 9. At the gas phase frequency, the calculated T_1 time is approximately 2 ps. This is in reasonably good agreement with the time determined by fitting the experimental data with the population master equation. The simulations indicate that the interactions causing HgI to relax vibrationally are short range in nature, and are dominated by the local rotational and librational modes of the solvent. These modes give rise to the large amplitude of the low frequency region of the spectrum (less than 200 cm^{-1}) of Fig. 9. The peaks in the 650, 1000 and 1450 cm^{-1} spectral regions correspond to the internal modes of ethanol. The solvent remained at equilibrium with the solute for all simulation times. Since the HgI vibrational frequency is comparable with the orientational time of the solvent, a non-equilibrium simulation may be required. This is due to the fact that the ethanol molecules do not have enough time to follow the HgI vibration adiabatically and an additional solvent coordinate is needed. It is also possible that the solvent may not be able to handle the rapid dissipation of vibrational energy and the energy may flow back into HgI.

3.4. Abstraction reactions

Another class of reactions that are ubiquitous in solution involves those that are diffusion controlled. The reactive part of such reactions, which occurs only when the combining molecules are close together, is of great interest. The study of bimolecular reaction dynamics in solution requires the creation of very special experimental conditions. We discuss the well-known stratagem of creating a transition state of the A + BA reaction by direct excitation of ABA, and give HgI_2 as an example. Another approach is to create the two reactants as neighboring molecules in solution by a fast photoreaction. For example, one of the reactants can be produced in a particular distribution of states by photolysis of a precursor. The precursor is dissolved in a solvent that consists of the other reactant. In this way, a reactive radical can be suddenly created within a van der Waals' separation of the molecules with which it is to react. The subsequent reaction is controlled by the forces between the reactants and the solvent influence on the dynamics.

Two reactions have been reported by this technique. One involved Cl atoms from the photolysis of Cl_2 in liquid chloroform, reacting with $HCCl_3$ molecules to produce HCl by hydrogen abstraction [1]. In the other, CN radicals, generated from the photolysis of ICN in chloroform, abstracted hydrogen to yield HCN and ClCN [2]. Transient infrared spectroscopy was employed to detect the rate of HCl or HCN formation and the vibrational state distributions in these products. Some essential features of the dynamics of the CN radical abstracting H from the C–H bond of $CHCl_3$ were examined recently using classical simulations [16]. The results of the experiments are not as expected on the basis of the behavior of the isolated molecules. For example, in solution, the time constant for HCN formation is 300 ps and is temperature insensitive, and the nascent vibrational state distribution is almost thermal. In contrast, in the gas phase, the reaction of thermal CN radicals with chloroform occurs on every collision, and a highly non-thermal (inverted) vibrational distribution in the C–H mode is generated [17]. The changed vibrational state distribution immediately tells us that the potential energy surface determining the forces on the atoms near the transition state is significantly modified by the solvent. The transition state region in the solution appears to be closer to the HCN product structure than in the gas phase. The other interesting fact is that the transitionally hot CN radicals generated in the ICN photolysis do not react with the adjacent chloroform molecules, but are simply cooled by the collisions. The simulations [16] show each CN radical to be solvated by about seven chloroform mole-

cules and provide a timescale for the translational cooling in the range of a few hundred femtoseconds. They also confirm that the slow rate of this barrierless reaction is a result of the improbability of the reactants achieving the transition state. This structure must therefore have a nearly collinear H–C–N configuration, with bond lengths closer to those in HCN.

These results show that a solution phase reaction can be diffusion controlled even though the reactants are at van der Waals' distances and there is no barrier. Diffusion-controlled reactions and caging effects have been studied by physical chemists for many years [18]. The effects of solvent caging, the distance and orientational dependence of reactivity [19] and hydrodynamic interactions [20] were examined by a variety of statistical methods. A dramatic difference between gas phase and solution phase reactivity, even for bimolecular reactions for which the diffusive encounter process itself is not the rate-limiting step, can be expected solely on the basis of the differences in rotational motion. In the gas phase, chloroform molecules at 300 K have a mean rotational period of 300 fs which is comparable with the period of a collision having an impact parameter of a few angstroms. In liquid chloroform, a molecule requires 12 ps to turn end-over-end by rotational diffusion, which is hundreds of times slower than the collision period. Clearly, the liquid structure and dynamics, as characterized by the translational and rotational diffusion parameters and the specific forces between reactants, can greatly influence the ability of the reactants to achieve the configurations necessary for reaction to occur. Only recently have the new techniques of ultrafast spectroscopy made it possible for experimentalists to probe the detailed predictions of statistical theories of diffusion-controlled reactions involving chemically anisotropic species. A next step must be the introduction of first principles quantum techniques into the theory in order to describe the potential surfaces on which the solute and nearby solvent molecules are moving.

Acknowledgements

This research was supported by grants from NSF and NIH.

References

[1] D. Raftery, M. Iannone, C.M. Philips and R.M. Hochstrasser, *Chem. Phys. Lett., 201* (1993) 513.
[2] D. Raftery, E. Gooding, A. Romanovsky and R.M. Hochstrasser, *J. Chem. Phys., 101* (1994) 8572.
[3] N. Pugliano, D.K. Palit, A.Z. Szarka and R.M. Hochstrasser, *J. Chem. Phys., 99* (1993) 7273.
[4] N. Pugliano, A.Z. Szarka, S. Gnanakaran, M. Treichel and R.M. Hochstrasser, *J. Chem. Phys., 103* (1995) 6498.
[5] N. Pugliano, A. Szarka and R.M. Hochstrasser, *J. Chem. Phys., 104* (1996) 5062.
[6] R.M. Bowman, M. Dantus and A.H. Zewail, *Chem. Phys. Lett., 156* (1989) 131.
[7] M. Dantus, R.M. Bowman, M. Gruebele and A.H. Zewail, *J. Chem. Phys., 91* (1989) 7437.
[8] M. Gruebele, G. Roberts and A.H. Zewail, *Philos. Trans. R. Soc. London A, 332* (1990) 223.
[9] I. Benjamin, P.F. Barbara, B.J. Gertner and J.T. Hynes, *J. Phys. Chem., 99* (1995) 7557.
[10] A.G. Redfield, in J.S. Waugh (ed.), *Advances in Magnetic Resonance*, Academic Press, New York, 1965, p. 1.
[11] C.P. Slichter, *Principles of Magnetic Resonance*, Springer, Berlin, 1990.
[12] C. Cohen-Tannoudji, J. Dupont-Roc and G. Grymberg, *Atom Photon Interactions*, Wiley Interscience, New York, 1992.
[13] S. Chandrasekhar, *Rev. Mod. Phys., 15* (1943) 1.
[14] J. Owrutsky, D. Raftery and R.M. Hochstrasser, *Ann. Rev. Phys. Chem., 45* (1994) 519.
[15] B.R. Brooks, R.E. Bruccoleri, B.B. Olafson, D.J. States, S. Swaminathan and M. Karplus, *J. Comp. Chem., 4* (1983) 187.
[16] I. Benjamin, *J. Chem. Phys., 103* (1995) 2459.
[17] V.R. Morris, F. Mohammad, L. Valdry and W.M. Jackson, *Chem. Phys. Lett., 220* (1994) 448.
[18] D.F. Calef and J.M. Deutsch, *Ann. Rev. Phys. Chem., 34* (1983) 493. R.M. Noyes, *Prog. React. Kinet., 1* (1961) 129.
[19] S. Lee and M. Karplus, *J. Chem. Phys., 86* (1987) 1908.
[20] P.G. Wolynes and J.M. Deutsch, *J. Chem. Phys., 65* (1976) 450.